NUMERICAL INVESTIGATION OF AERODYNAMICS AND ACOUSTICS OF RIGID MAIN ROTOR IN FORWARD FLIGHT

I. Abalakin, V. Bobkov, T. Kozubskaya

veld13@gmail.com, Keldysh Institute of Applied Mathematics, Russian Federation

B. Kritsky, R. Mirgazov, V. Vershkov,

ruslan.mirgazov@tsagi.ru, Central Aerohydrodynamic Institute, Russian Federation

Abstract

The paper is devoted to the numerical simulation of the flow near the rigid helicopter rotor in the forward flight mode using the Reynolds-averaged Navier-Stokes equations in the rotating non-inertial reference frame. The numerical method is based on the vertex-centered EBR scheme for unstructured hybrid meshes. The computations are performed using the in-house code NOISEtte and the software package ANSYS CFX. The numerically obtained aerodynamic characteristics of the rotor are comparatively analyzed against the results of full-scale experiments.

1. INTRODUCTION

The helicopter development is mostly aimed at the improvement of its flight performance characteristics such as rotor thrust, drag coefficient, fuel efficiency, air speed, etc. For this purpose, it is important to have the detailed information about the flow generated around the vehicle and its influence on the design and behavior of the aircraft. In the modern helicopter industry, in order to obtain the required data at the design stage, along with experiments in wind tunnels, the numerical simulations on high-performance computing systems are widely used. In particular, such approach allows us to predict and analyze the aerodynamic characteristics of a helicopter in advance and thereby to reduce the time and costs of developing the helicopter.

The simulation of flow around a helicopter presents a serious difficulty because of the need to consider numerous interacting factors. So the accuracy of the numerical methods and codes must be carefully verified and validated by comparing both with the experimental data and results obtained using different methods and software packages.

In the paper, in order to validate the developed method of numerical simulation of flow around a helicopter rotor [1], we consider the rigid model rotor in the forward flight mode. We compare our results obtained using the in-house code NOISEtte [2] with the available experimental data of TsAGI and the numerical results of software package ANSYS CFX.

The main feature of numerical method presented in the paper is the usage of lower-cost higher-accuracy vertex-centered scheme for unstructured hybrid meshes. The ability to work effectively on hybrid unstructured meshes greatly simplifies the mesh generation with a flexible adaptation of the mesh to the complex blade geometry. The higher accuracy of numerical results obtained on such meshes is provided by using the EBR (Edge-Based Reconstruction) scheme [3-5] based on a quasi-1D edge-oriented approximations of inviscid flows.

2. PROBLEM FORMULATION

The geometry under consideration (Fig. 1) completely corresponds to the rotor configuration experimentally tested at TsAGI. It presents the helicopter rotor with four blades rigid in bending and torsion. The blades are rectangular in

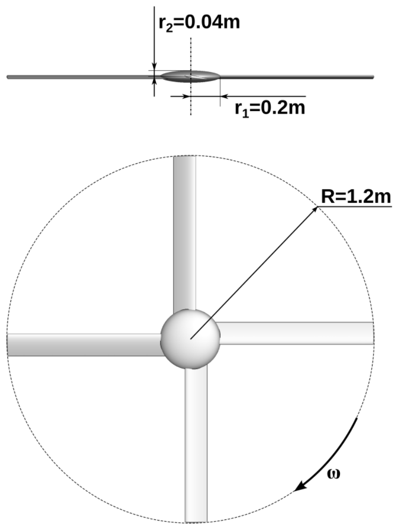

Fig.1. Rotor geometry.

Presented at 45th European Rotorcraft Forum, Warsaw, Poland, 17-20 September, 2019

planform with a NACA0012 airfoil shape without twist. The total blade pitch angle is 8°. The blades have the chord of $b = 0.15$ m. The radius of the blade root is $r_0 = 0.2$ m with the total rotor radius equal to $r_0 = 1.2$ m. The hub is an ellipsoid having the horizontal and vertical radii of $r_1 = 0.04$ and $r_2 = 0.2$ m respectively.

The rotation velocity ω is equal to 360 rpm corresponding to the blade tip speed $V_{tip} = 45.24$ m/s. The flow near the helicopter rotor is simulated with three various free-stream velocities $V_{flow} = 6.79, 11.31, 20.36$ m/s with zero angle of attack. The free-stream parameters correspond to the standard conditions under which the temperature is 23°C, the pressure is 103025 Pa, the density is $\rho_0 = 1.225$ kg/m^3, the dynamic viscosity is $\mu_0 = 1.827\times10^{-5}$ Pa·s. These parameters determine the Reynolds number $\mathrm{Re} = \rho_0 V_{tip} b / \mu_0 = 4.55\cdot10^5$.

3. THE CHARACTERISTICS UNDER STUDY

3.1. Rotor aerodynamic forces

The main parameters characterizing the configuration under study are the aerodynamic forces represented by the thrust, longitudinal torque and normal force coefficients.

The thrust and longitudinal torque coefficients are calculated through the projection of force acting on the rotor blades in the absolute fixed reference frame

$$c_T = \frac{2N}{\rho_0 A(\omega R)^2}\int_S p n_z ds,$$
$$m_x = \frac{2N}{\rho_0 R A(\omega R)^2}\int_S p\left(n_z y - n_x z\right) ds. \tag{1}$$

Here N is the number of the blades, p is the pressure distribution over the blade surface *S*, and n_x, n_y, and n_z are the projections of unit normal outward with respect to the surface *S* specified in the absolute fixed reference frame, ρ_0 is the undisturbed flow density, $A = \pi R^2$ is the blade disk area.

The normal force coefficient is evaluated for the blade normal section defined by the curve *L*

$$c_n = \frac{2}{\rho_0 A(\omega R)^2}\int_L p n'_z \, dl, \tag{2}$$

where $n'_z = n_x \cos\varphi - n_y \sin\varphi$ is the component of blade-surface unit normal in the blade axis system.

3.2. Acoustic characteristics

An important acoustical characteristic of a flow is the overall sound pressure level (OASPL) in the far field which is determined by the far-field pressure fluctuation spectrum $P(\mathbf{x}, f)$. The pressure fluctuation spectrum is given by the Fourier transform of the function $p'(\mathbf{x},t)$ normalized by the quantity $p_0 = 2\times10^{-5}$ Pa

$$P(\mathbf{x}, f) = \frac{1}{\sqrt{2\pi}}\int_{-\infty}^{\infty}\frac{p'(\mathbf{x},t)}{p_0}e^{-i2\pi f} dt.$$

We determine the total energy of the spectrum as the integral of the spectral power $S(\mathbf{x}, f) = P^2(\mathbf{x}, f)$

$$E(\mathbf{x}) = \int S(\mathbf{x}, f) df,$$

where the integration is performed over all resolvable frequencies. Then the OASPL expressed in decibels is determined from the formula

$$\mathrm{OASPL} = 10\log_{10} E(\mathbf{x}).$$

4. MATHEMATICAL MODEL

4.1. Navier-Stokes equations in a non-inertial reference frame

To simulate the external flow around the rotor with the rotational speed $\boldsymbol{\omega}$, the Reynolds-averaged Navier-Stokes (RANS) equations for compressible gas with the Spalart-Allmaras turbulence model are used. The equations system is considered in the non-inertial rotating reference frame. The reference frame rotates around the fixed rotor axis with the constant angular velocity equal to the rotational speed. This means that the blades streamlined by the gas flow are immovable, and the direction of external flow varies depending on the azimuth angle $\psi(t) = -|\boldsymbol{\omega}|t$.

The Navier-Stokes equations in the non-inertial reference frame are given in [1]. In the paper, we consider the RANS model with the Spalart-Allmaras evolution equation

$$\frac{\partial\rho\tilde{\nu}}{\partial t} + \frac{\partial\rho\tilde{\nu}u_i}{\partial x_i} = D_\nu + G_\nu - Y_\nu.$$

The definition of terms D_ν, G_ν, Y_ν describing, respectively, the diffusion, generation and

Presented at 45th European Rotorcraft Forum, Warsaw, Poland, 17-20 September, 2019

dissipation of turbulence can be found, for example, in [6].
The value $\tilde{\nu}$ is used to calculate the turbulent viscosity coefficient μ_T as

$$\mu_T = \rho\tilde{\nu}\frac{\chi^3}{\chi^3 + 357.911}, \quad \chi = \frac{\rho\tilde{\nu}}{\mu}.$$

4.2. Boundary conditions

4.2.1. Solid wall boundary conditions based on wall functions

In all the predictions, in order to reduce costs, we use rather coarse meshes in the near-wall region so that the noslip boundary conditions may result in an incorrect determination of velocity gradients on the solid wall. Instead of the noslip condition, we use the analytically predicted velocity distribution in the turbulent boundary layer. This approach determines the boundary-wall function simulating the flow in the unresolved part of boundary layer [7]. The implementation of wall functions depends on the discretization method we use for the Navier-Stokes equations.
Let u_* is the friction velocity determined by the wall stress τ_w and the wall density ρ_w

(3) $$u_* = \sqrt{\frac{1}{\rho_w}\tau_w}$$

and $y^+ = \rho u_* h_{nw}/\mu$ is near-wall Reynolds number. Here h_{nw} is the characteristic size along the normal to the solid surface of near-wall cells.
Determine the viscous component of momentum flux $\mathbf{F}_w^{wl}$ on the boundary surface through the wall stress. Taking into account the relation (3) it can be expressed as

(4) $$\mathbf{F}_w^{wl} = \rho u_*^2 \mathbf{u}_t^e,$$

where $\mathbf{u}_t^e$ is the unit vector of tangential velocity on the boundary surface equal to

$$\mathbf{u}_t^e = \mathbf{u_t} / |\mathbf{u_t}|, \qquad \mathbf{u_t} = \mathbf{u} - u_n\mathbf{n}$$

and u_n is the normal speed on the boundary surface which is equal to the normal component of wall velocity $V_n = (\boldsymbol{\omega}\times\mathbf{r})\cdot\mathbf{n}$.
Thus, to determine the viscous flux component, we need to know the friction velocity. It can be found by solving the following nonlinear equation

(5) $$|\mathbf{u}_t| - u_* f\left(\frac{u_*\rho h_{nw}}{\mu}\right) = 0, \quad y^+ = \frac{\rho u_* h_{nw}}{\mu}$$

where the boundary-wall function $f(y^+)$ determining the velocity profile in the viscous, buffer, and logarithmic sublayers is given by the Reichardt law [8]

$$f(y^+) = \frac{1}{0.41}\ln(1 + 0.41y^+) + 7.8\left(1 - e^{-\frac{y^+}{11}} - \frac{y^+}{11}e^{-\frac{y^+}{3}}\right).$$

Equation (5) is solved by the Newton method. At each iteration of it, the values $\mathbf{u}_t$, μ, ρ are taken at the nodes of boundary surface. The initial guess of friction velocity is chosen as $u_f^0 = \tau_w^0 / |\mathbf{u}_t|$ where the wall stress is calculated through the normal derivative of the tangential velocity magnitude using the first difference

$$\tau_w = \mu\frac{|\mathbf{u}_t|}{\delta}.$$

The value $\delta = h_w / 2$ is determined as the distance to the solid wall where the noslip conditions are valid. The tangential velocity magnitude is taken on the boundary surface.
The resulting expression for the momentum flux vector on the boundary surface represents the sum of the flux (4) and the convective flux component $(u_n - V_n)\mathbf{u} + p\mathbf{n}$ taking into account the condition $u_n = V_n$

$$\mathbf{F}_w = p\mathbf{n} + \mathbf{F}_w^{wl}.$$

4.2.2. Conditions on external boundaries

Since the numerical simulation is performed in a bounded region, some artificial boundary conditions must be imposed on the boundary of computational domain.
These boundary conditions are determined by splitting the fluxes relating the values of the gasdynamic parameters within the computation domain and their values in the distant flow in the directions of characteristic velocities. The latter values are determined by the characteristic relations for an isentropic gas [1].

5. NUMERICAL METHOD

5.1. Numerical method for simulating the near flow field

The method for simulating the near flow field is based on the Navier-Stokes equations considered in the rotating non-inertial reference frame. The space approximation is built in the vertex-centered framework when the variables are defined in the hybrid mesh vertices. According to the finite-volume approach, the conservation laws are formulated for the dual cells, i.e. the control volumes specially built around the vertices. The numerical flux through the dual cell faces is calculated by the Roe approximate Riemann solver. The higher accuracy of the numerical scheme is achieved thanks to the quasi-1D edge-oriented reconstructions of variables involved in the flux calculation. The resulting EBR (Edge

Presented at 45th European Rotorcraft Forum, Warsaw, Poland, 17-20 September, 2019

Based Reconstruction) scheme is described in detail in [3-5].
On translationally invariant (TI) tetrahedral or hexahedral meshes, i.e. uniform grid-like meshes, the EBR scheme provides the high (up to the 5^{th}-6^{th}) order of approximation accuracy of a smooth solution if the quasi-1D reconstruction is applied to the flux variables [4, 5]. Despite the fact that on arbitrary hybrid unstructured meshes this scheme has theoretically the second order, it provides a noticeably higher accuracy in terms of error values in comparison with the traditional Godunov-type finite-volume schemes of the second order [4].
To approximate the viscous terms of Navier-Stokes equations, we use the Galerkin method with linear basic functions.
The implicit three-layer second-order scheme with the Newton linearization is used for the time integration. At each Newton iteration, the resulting system of linear equations is solved by the stabilized bi-conjugate gradient (BiCGStab) method [9].
The mentioned numerical algorithms are implemented in the in-house code NOISEtte [2].

5.2. Computational domain and meshes

In all the considered cases, the computational domain has a form of cylinder with the radius of 10 rotor radii. The cylinder axis coincides with the helicopter rotation axis. The lower boundary of the computational domain is located at the distance of 15 rotor radii from the plane of rotation, and the upper boundary is at the distance of 10 radii.

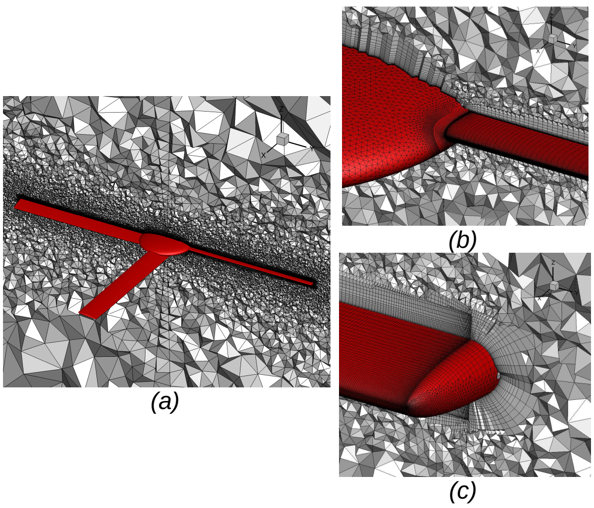

Fig.2. Computational mesh.

The computational domain is filled with the hybrid unstructured mesh with refining in the regions where the detailed representation of flow structure is required. Thus, the finest tetrahedral mesh is built at the leading and trailing blade edges, at the blade tip and at the region of blade junction to the central body (Fig. 2b, c). The blade surface is framed by the prismatic mesh layers with the exponentially increasing height. When the initially anisotropic prisms become close to isotropic, the mesh goes to a quasi-uniform tetrahedral unstructured form with a smooth coarsening towards the outer boundaries of computational domain (Fig. 2a).
The resulting mesh consists of 9.3M nodes and 24.3M elements.
The mesh was generated using ANSYS ICEM CFD [10].

5.3. Numerical method for calculating the far field acoustics

The integral formulation "1A" of the Ffowcs Williams- Hawkings (FWH) method proposed by Farassat [11] is used for estimating the acoustic characteristics of the model helicopter rotor in forward flight. The "1A" formulation supposes the use of a control surface of an arbitrary shape so that the velocity in the control-surface points is assumed to be subsonic. Otherwise, when passing over the speed of sound, the integral formula contains a singularity that makes it difficult to apply the FWH for a rotating rotor. Some solutions of this problem are proposed in [12, 13]. However, their implementation is quite complicated and entails significant additional computational costs. A rather simple and efficient way to implement the modification of "1A" formulation for a helicopter rotor is proposed in [14]. The key idea of this modification is the parametrization of control surface in the absolute reference frame associated with the helicopter fuselage and not in the non-inertial rotating reference frame associated with the rotor. It is required that the control surface must be a surface of revolution about the axis of the rotor. This assumption keeps the surface non-deforming under the proposed parametrization. In addition, the use of a uniform surface mesh in spherical coordinates provides a simple procedure of the variables interpolation and the corresponding calculation of the angular derivatives at each point laying on the control surface. As a result, the problem reduces to calculating the surface integral with delay basing on the necessary data on the surface moving with respect to the background flow.

6. RESULTS

In a forward flight, the shape of vortex wake behind the rotor is complex and non-uniform. The strongly disturbed flow also includes the tip vortices. Their shape depends on the curvilinear motion of blades characterized by the ratio

Presented at 45th European Rotorcraft Forum, Warsaw, Poland, 17-20 September, 2019

between the upstream and rotating velocities, and the number of blades. Without interactions, the shape of tip vortices would coincide with the trajectories of blade tips.

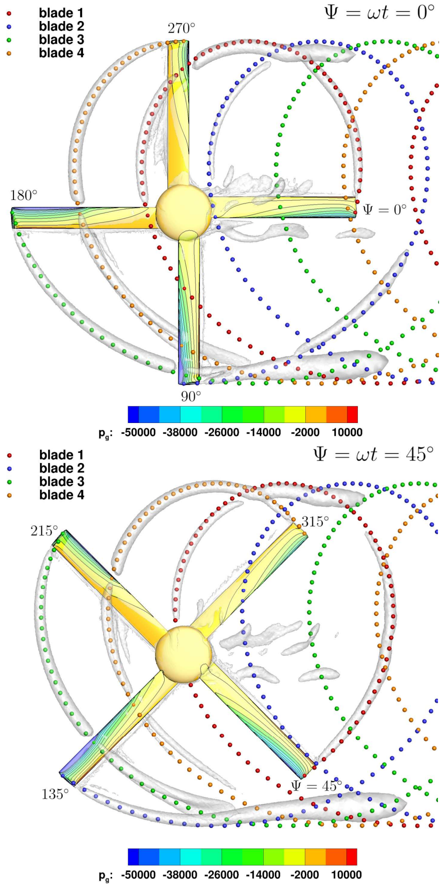

Fig.3. Tip vortices trajectories (rotor gauge pressure field and Q-criterion isosurfaces)

The flow around the rotor is characterized by the interaction of blades and turbulent structures. Due to the presence of upstream flow and rotational motion of the blades, the distribution of pressure on the surface of blade essentially depends on its azimuthal position. We evaluate the aerodynamic characteristics versus the azimuth angle and their distributions for some fixed azimuthal positions of the rotor.

The overall flow pattern is determined by the tip vortices that break away from the blades, drift downstream and interact both with the incident blades and turbulent structures. The position of tip vortices cores follows the trajectories of motion of the blades' tips taking into account the rotation and the drift by the upstream flow. This can be observed in Fig. 3 where the visualization of vortices by the multiply connected isosurface of Q-criterion [15] is given at the fixed times corresponding to the azimuthal angles and trajectories of blades' tips in the absolute reference frame in the rotation plane. The trajectories of the blades' tips are defined by the following law:

$$\begin{pmatrix} x \\ y \end{pmatrix} = \begin{pmatrix} R\cos(\omega t + \psi_k) - tV_{flow} \\ R\sin(\omega t + \psi_k) \end{pmatrix}, \; k = 0,\ldots,3$$

where $\psi_k = (\pi/2)k$ – are the initial azimuthal angles of corresponding blades.

The aerodynamic characteristics of rotor are determined by the pressure distribution on the blade surface (see formulas (1), (2)).

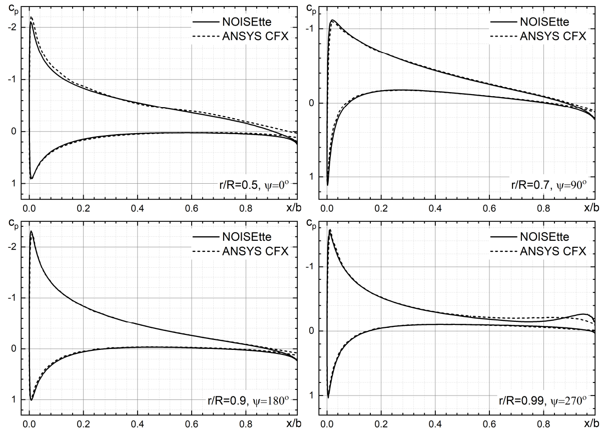

Fig.4. Pressure coefficient distributions

The pressure coefficient distributions obtained using the code NOISEtte and software package ANSYS CFX (Fig. 4) are in good agreement with each other for all the cross sections and azimuth angles. The slight discrepancy in the values of pressure coefficient near the blade trailing edge is explained by the different resolution of the surface mesh in this area.

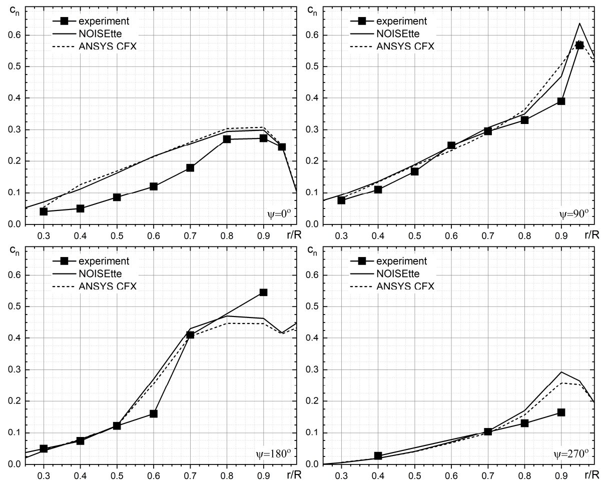

Fig.5. Normal force coefficient distributions

The distributions of normal force coefficient over the blade span obtained in computational experiments for different azimuthal positions of the blades shown in Fig.5 also agree well with each other. One can see the characteristic drop in the operational efficiency of retreating blade in the range of azimuth angles of 270° - 360°(0°) which is expectable at the forward flight mode. A slight difference in comparison with the experimental data is supposedly caused by the system error in measuring the azimuthal position of the blade in the experiment. This is indirectly confirmed by the presence of a similar shift along the azimuth angle observed when comparing the numerical and experimental measurements of pressure differences in the region of blade leading edge (Fig.6). These plots show the dependence of pressure difference measured at the points near the blade leading edge on the azimuthal position of blade (Fig.6a). Taking into account the above-mentioned shift in azimuth angle, this value obtained in the computational experiment agrees well with the experiment (see Fig.6b, c).

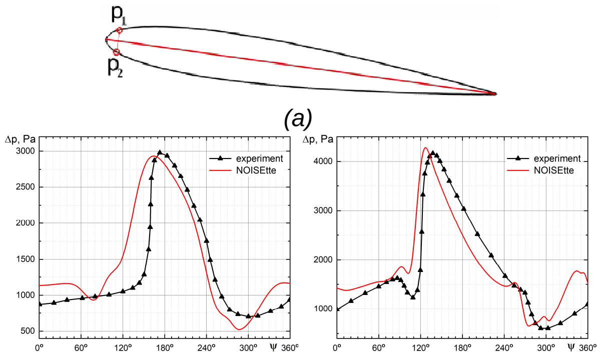

(a)

(b) (c)

Fig.6. Pressure difference p_2-p_1 (a) for flight velocity 6.8 m/s (b) and 11.3 m/s (c)

The values of lift coefficients and longitudinal torque obtained by the two codes (Fig.7) are close for all the azimuth angles.

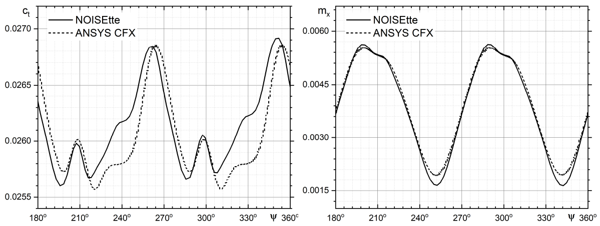

(a) (b)

Fig.7. Thrust (a) and torque (b) coefficients

Basing on the pressure pulsation history accumulated in the near field and following the strategies described in sections 5.3 and 3.2, we build the directivity diagram of the acoustic radiation in the far field (Fig.8). The expected maximal values of sound pressure level are observed both upstream and downstream in the rotation plane.

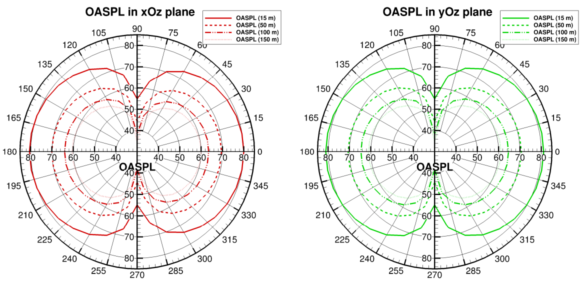

(a) (b)

Fig.8. Overall sound pressure level directivity diagram

The computations have been carried out by the in-house code NOISEtte using 200-480 CPU cores within two-level MPI+OpenMP parallel model [2].

7. CONCLUSION

The paper presents the results of numerical simulation of turbulent flow around the model four-blade helicopter rotor in forward flight. The validation of the developed numerical method implemented in the in-house code NOISEtte has been carried out by comparing with the numerical results obtained by ANSYS CFX and experimental data.

The comparison of aerodynamic characteristics such as the distribution of pressure and normal-force coefficients and their dependencies on the azimuth angle shows a rather good agreement.

Besides, basing on the numerical data in the near-field flow we have evaluated the sound radiation generated by the rotor in the far field. The acoustic results look reasonable, however can not be evaluated in the full measure due to the absence of experimental or reference numerical data to compare with.

The work has been funded by the Russian Science Foundation, project 19-11-00299

The results have been obtained using the computational resources of MCC NRC “Kurchatov Institute” [16].

REFERENCES

1. I. V. Abalakin, V. A. Anikin, P. A. Bakhvalov, V. G. Bobkov, and T. K. Kozubskaya. Numerical Investigation of the Aerodynamic and Acoustical Properties of a Shrouded Rotor // Fluid Dynamics, 2016, V. 51, No. 3, P. 419-433.
2. I. V. Abalakin, P. A. Bakhvalov, A. V. Gorobets, A. P. Duben', and T. K. Kozubskaya. NOISEtte Parallel Software Package for Large-Scale Calculations of Problems in Aerodynamics and Aeroacoustics // Numerical methods and Programming, 2012, V. 13, No. 2, P. 110-125 (in Russian).
3. Abalakin I., Bakhvalov P., Kozubskaya T. Edge-based reconstruction schemes for prediction of near field flow region in complex aeroacoustics problems // Int. J. Aeroacoust, 2014, V. 13, No. 3-4. P. 207-234. (10)
4. Abalakin I., Bakhvalov P., Kozubskaya T. Edge-based reconstruction schemes for unstructured tetrahedral meshes // Int. J. Numer. Meth. Fluids. 2016. V. 81, No. 6. P. 331-356. (11)
5. P. A. Bakhvalov. Quasi one-dimensional reconstruction scheme on convex polygonal meshes for solving aeroacoustics problems // Mathematical Models and Computer Simulations, 2016, V. 6, No. 2, P. 192-202. (12)
6. Spalart P. R., Allmaras S. R. A One-Equation Turbulence Model for Aerodynamic Flows // 30th Aerospace Sciences Meeting and Exhibit, Aerospace Sciences Meetings, AIAA Paper No. 1992-0439, 1992.
7. Wilcox D.C. Turbulence Modeling for CFD, Third edition. La Cañada, California: DCW Industries, 2006. 522 p.
8. Reichard H. Vollständige Darstellung der turbulenten Geschwindigkeitsverteilung in glatten Leitungen // ZAMM – Journal of Applied Mathematics and Mechanics / Zeitschrift für Angewandte Mathematik und Mechanik, 1951, Bd. 31, S. 208-219.
9. Saad Y. Iterative methods for sparse linear systems. Philadelphia: Society for Industrial and Applied Mathematics, 2003. P. 528.
10. ANSYS, Inc. ANSYS. 1970-2018, https://www.ansys.com.
11. Farassat, F. Derivation of formulations 1 and 1A of Farassat. NASA Technical Memorandum 2007-214853, NASA, Langley Research Center, Hampton, Virginia, March 2007.(7)
12. Farassat, F. and Myers, M. K. The Kirchhoff formula for a supersonically moving surface. First CEAS/AIAA Aeroacoustics Conference (16th AIAA Aeroacoustics Conference), Munich, Germany, June 12-15, AIAA Paper 95-062, 1995. (8)
13. Farassat, F., Brentner, K. and Dunn, M. A study of supersonic surface sources the Ffowcs Williams-Hawkings equation and the Kirchhoff formula. 4th AIAA/CEAS Aeroacoustics Conference, Toulouse, France, June 2-4, AIAA Paper 98-2375, 1998. (9)
14. P. A. Bakhvalov, V. G. Bobkov, and T. K. Kozubskaya. Technology to predict acoustic far fileld disturbances in the case of calculations in a rotating reference frame // Mathematical Models and Computer Simulations, 2017, V. 9, No. 6, P. 717-727. (10)
15. Cucitore R., Quadrio M., Baron A. On the effectiveness and limitations of local criteria for the identification of a vortex // Eur. J. Mech. B/Fluids. 1999. V. 18, № 2, P. 261-282
16. MCC NRC "Кurchatov Institute", http://computing.nrcki.ru/

Presented at 45th European Rotorcraft Forum, Warsaw, Poland, 17-20 September, 2019